

# Eu<sup>3+</sup> optically detected nuclear quadrupole resonance in stoichiometric europium vanadate

R. L. Cone,\* P. C. Hansen, and M. J. M. Leask

Clarendon Laboratory, Parks Road, Oxford OX1 3PU, UK

Received October 15, 1991; revised manuscript received December 16, 1991

Defect Eu<sup>3+</sup> sites in EuVO<sub>4</sub> have been studied with the high-resolution techniques of spectral hole burning and optically detected nuclear quadrupole resonance. A number of EuVO<sub>4</sub> crystals prepared from fluxes with various compositions have been used to show that some point defects are associated with specific chemical impurities but that other defects seem to be present even in the purest crystals. Site-dependent nuclear quadrupole parameters  $P$  and  $\eta$  have been determined for both <sup>7</sup>F<sub>0</sub> and <sup>5</sup>D<sub>0</sub> states at two defect sites, and the nuclear Zeeman effect has permitted the local defect site principal axes to be determined.

## INTRODUCTION

Previous studies<sup>1-4</sup> of stoichiometric europium vanadate, EuVO<sub>4</sub>, have revealed that there are a surprisingly large number of crystallographically perturbed (defect) Eu<sup>3+</sup> sites in even high-quality single crystals. This paper reports our continued efforts to catalog and to explore the nature and origins of these defects in EuVO<sub>4</sub> and related stoichiometric and doped Eu<sup>3+</sup> compounds.

Laser excitation in the Eu<sup>3+</sup>:<sup>7</sup>F<sub>0</sub> → <sup>5</sup>D<sub>0</sub> region (580 nm) of EuVO<sub>4</sub> shows more than 40 lines spread over some 40 cm<sup>-1</sup>. Each of these lines must be due to a distinct type of defect site in the crystal structure, since the transition  $J = 0 \rightarrow J = 0$  has no crystal field splittings and is also strictly forbidden at the intrinsic ( $D_{2d}$  symmetry) Eu<sup>3+</sup> sites in EuVO<sub>4</sub>. The intrinsic site transition does, however, become allowed in an applied magnetic field, and it has been located at 17 196.7 cm<sup>-1</sup> in all EuVO<sub>4</sub> crystals studied so far.

A detailed survey of excitation spectra obtained from many EuVO<sub>4</sub> crystals prepared from a variety of starting fluxes has shown that, while such spectra differ in detail, several major defect lines are likely to be a natural characteristic of EuVO<sub>4</sub> itself rather than of the specific crystal growth procedure. Almost all of the defect lines are amenable to cw spectral hole burning and optically detected nuclear quadrupole resonance (ODNQR) using a single-frequency Coherent CR599-21 tunable dye laser, and that tractability has permitted such lines to be characterized in terms of the site-dependent quadrupole parameters  $P$  and  $\eta$  that describe the quadrupole splittings in the  $I = 5/2$  states of the isotopes <sup>151</sup>Eu and <sup>153</sup>Eu.<sup>1-5</sup>

Detailed information has been obtained on many defect sites in EuVO<sub>4</sub>, but to date none has been fully described. Zeeman experiments, involving both the electronic transitions and the hole-burning spectra, have been useful in establishing the directions of the local principal axes at defect sites relative to those of the crystal. Also, variations in flux growth materials have shown that some prominent defects occur only when fluorides are present in the flux, presumably leading to either interstitial or substitutional defects involving F<sup>-</sup> ions. Extraction of further detail, however, presents a challenge. The polar-

ization of the Eu<sup>3+</sup> defect optical transitions, for example, generally ranges from moderate polarization anisotropy to an almost complete lack of polarization dependence; that is, defect site symmetries are sufficiently low that clear-cut selection rules do not exist and do not permit deductions to be made on that basis, as in other systems that have been studied previously.<sup>5</sup>

The present work focuses attention on detailed analyses of the line at 516 635 GHz, which we subsequently refer to as line 41 from crystal growth I, and the line at 515 980 GHz, which we subsequently refer to as line 44 from growth A (see Ref. 3 and 4 for details of these and other crystal growths). Line 41 is almost certainly associated with the presence of F<sup>-</sup>, while line 44 appeared in growth A, which was an attempt to produce EuVO<sub>4</sub> crystals of high purity. Both these lines have been studied here by rf ODNQR techniques, leading to high precision in the quadrupole parameters  $P$  and  $\eta$  but also to dramatically different results for the defect site values of the Eu<sup>3+</sup> <sup>7</sup>F<sub>0</sub> nuclear shielding parameter  $\alpha$  as compared with the values calculated for the intrinsic site.

## EXPERIMENTAL PROCEDURE

Previous papers<sup>1-4</sup> on EuVO<sub>4</sub> have given a detailed description of the spectroscopic and laser hole-burning techniques, so only a brief outline will be given here. The Eu<sup>3+</sup> defect excitation spectra in the <sup>7</sup>F<sub>0</sub> → <sup>5</sup>D<sub>0</sub> region were excited by a Coherent CR599-21 dye laser operating on Rhodamine 6G and were recorded by monitoring the red fluorescence emission arising from the transitions <sup>5</sup>D<sub>0</sub> → <sup>7</sup>F<sub>1,2</sub>. Hole burning of individual defect lines was achieved with identical burn-beam and read-beam intensities produced by the CR599-21 laser, running narrow band (~2-MHz linewidth); the frequency scan rate during the read cycle was chosen to reduce the laser perturbation of the sample. Excitation wavelengths were measured with a double Michelson interferometer referenced to a He-Ne laser, giving an accuracy of ±2 GHz. The EuVO<sub>4</sub> crystals were always immersed in liquid helium at 1.5 K in the same helium bath as the 9-T radial-access superconducting magnet.

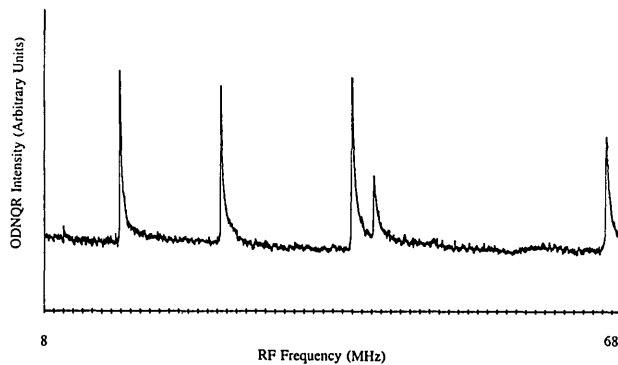


Fig. 1. ODNQR spectrum for line 44 (515 980 GHz) in  $\text{EuVO}_4$  in zero magnetic field. The resonances were all assigned to  ${}^7F_0$ . The asymmetric line shape is explained in the text.

For the ODNQR experiments the hole-burning setup was augmented by the addition of a computer-controlled rf signal generator, rf power amplifier, and rf probe enclosing the sample. The technique was identical with those used in a variety of double-resonance experiments: First the electronic transition was saturated; next changes in the degree of saturation were detected as the rf frequency was swept through the range corresponding to transitions between nuclear sublevels.<sup>5</sup> In this case saturation was achieved by locking the dye laser frequency at the center of a particular defect line. It was easy to carry out ODNQR on all lines that exhibited hole burning, and these encompassed almost all defect lines, as we noted above. A major source of signal amplitude noise arose from laser frequency jitter ( $\sim 2$  MHz), which caused transient burning of adjacent holes of varying depths; signal averaging reduced these amplitude fluctuations, so that changes in the level of saturation as a function of rf frequency were clearly observable, as shown in Fig. 1.

The  $\text{EuVO}_4$  crystal was mounted in a traveling-wave rf probe built for these experiments. The probe was assembled by using a five-turn coil and three small capacitors, chosen so that the distributed capacitor/coil arrangement had a characteristic impedance of  $\sim 50 \Omega$ . The coaxial line beyond the probe was terminated in a 50-W, 50- $\Omega$  load impedance. The probe's impedance match was somewhat less than perfect over the comparatively wide frequency range used in the experiments (250 kHz to 150 MHz), but the consequent slow variations in power did not cause problems.

The rf source was a digital Adret Electronique 740A signal generator, amplified by a 50-W Marconi TF 2167 broadband amplifier. For some of the experiments a more powerful 200-W ENI 3100LA amplifier was used. The maximum undistorted rf voltage measured across the rf coil (at room temperature) was typically 10 V peak-to-peak, corresponding to a maximum field at the sample position of  $\sim 5$  G as measured with a search coil. The use of a digital rather than an analog rf signal generator offered far greater flexibility in control, but it also introduced problems specific to its speed of control and operation.

The experiments were controlled from an IBM PC AT microcomputer with an internal IEEE-488 interface and a fast analog-to-digital converter, providing 12-bit signal resolution. The computer could step the frequency through the chosen range at a predetermined increment and record data from the photomultiplier detection system

through the analog-to-digital converter. A method of data collection involving one sample per frequency step and many scans over the chosen frequency range proved more successful than the alternative of collecting many samples per frequency step and making just one scan across the chosen range. This was because the application of resonant rf radiation to the system produced a transient rather than steady-state change, doubtless because of the relaxation times characterizing the dynamics of the optical pumping and the nuclear spin relaxation processes. Figure 1 shows a typical ODNQR result for line 44 (515 980 GHz) in zero magnetic field. It can be seen that (i) the signal-to-noise ratio is excellent and that (ii) the resonant peaks are asymmetric, with a pseudo-exponential decay to higher frequency. This effect was studied extensively, but the important point for the present study is that, when the frequency was scanned in the reverse direction (that is, from high to low in Fig. 1), the peaks were at exactly the same frequencies, but the pseudo-exponential decay was to the lower-frequency side, that is, in the direction opposite to that shown in Fig. 1. The peak frequencies were therefore unambiguously determined by a scan in just one direction, but it was obviously not possible to estimate the true resonance linewidth from such data.

For further investigation of that line-shape effect, a technique that used the full digital potential of the Adret signal generator was developed as follows. A scan range from  $f_1$ , just below the transition, to  $f_2$ , just above the transition, was noted, and a frequency  $f_0$  well below the region of interest was selected. ( $f_0$  was set at 11.000 MHz, for example, in a study of an ODNQR resonance at 11.535 MHz.) A frequency increment  $\Delta$  was used for the scan. The rf frequency was initially set to  $f_0$ . A frequency-jumping procedure was adopted so that the rf jumped from  $f_0$  to  $f_1$ , and a reading was taken; the rf then jumped back to  $f_0$  and paused for a set period ( $\sim 1$  s). Then it jumped to  $f_1 + \Delta$ , a new reading was taken, and the rf jumped back to  $f_0$ . The smash and grab procedure was repeated until  $f_1 + n\Delta$  reached the frequency  $f_2$ . The entire scan was repeated several times, and the results were averaged as before. This procedure was completely successful in that it revealed a symmetric line shape with a full width at half-maximum of  $\sim 60$  kHz for the particular resonance being studied (11.535 MHz). However, the procedure was quite time consuming because of the 1-s dwell time at  $f_0$  between increments; so, having succeeded in demonstrating that the asymmetric line shapes were an artifact of measurement, we did not use the procedure further.

## RESULTS AND DISCUSSION

### Zeeman Hole-Burning Spectra

For any particular defect site the orientation of the local principal axes relative to the crystallographic axes of the vanadate structure is important in the analysis of the corresponding ODNQR Zeeman spectra. For both lines 41 and 44 being discussed here this information was obtained initially from the effect of magnetic field on the hole-burning spectra, with the field being applied parallel to either the *a* or the *c* crystallographic axes.

The effect of the nuclear quadrupole interaction on the  $I = 5/2$  states in  $\text{Eu}^{3+}$  is to produce three nuclear Kramers

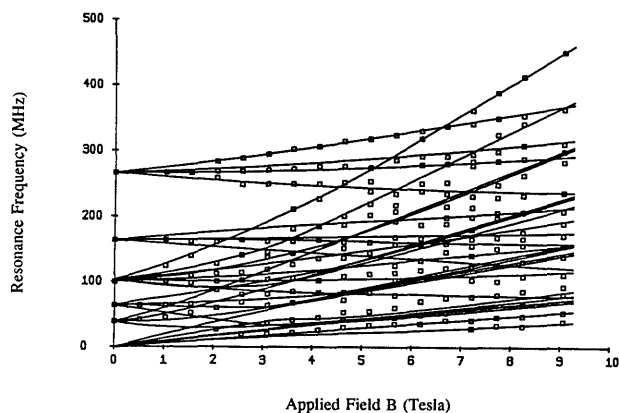


Fig. 2. The  ${}^5D_0$  Zeeman effect of the spectral hole burning for line 41 with the magnetic field  $\mathbf{B}$  applied parallel to the crystallographic  $c$  axis (squares). The theoretical fit (solid lines) was made by using the quadrupole parameters  $P$  and  $\eta$  along with the angles  $\theta$  and  $\Phi$  that specify the orientation of the applied field in the local defect coordinate system.

doublet states at different energies. For energy splittings A and B between these three states, previous research<sup>1-7</sup> shows that the hole-burning spectrum will contain *three* holes, corresponding to energies A, B, and A + B in the optically excited state. In addition, there are 21 antiholes, which have energies that are determined by linear combinations of both ground and optically excited state nuclear splittings A and B. Since there are two isotopes,  ${}^{151}\text{Eu}$  and  ${}^{153}\text{Eu}$ , the hole-burning spectrum will display at most 6 holes and 42 antiholes.

With an applied magnetic field the nuclear quadrupole Hamiltonian takes the form<sup>1-7</sup>

$$H = P \left( I_z^2 - \frac{35}{12} \right) + \frac{P\eta}{6} (I_+^2 + I_-^2) - \mu_B g_I \sum_{i=1}^3 (1 - \alpha_i) I_i B_i, \quad (1)$$

where  $P$  and  $\eta$  are the nuclear quadrupole parameters and  $\alpha$  is the (direction-dependent) nuclear shielding parameter, defined as

$$\alpha_i = 4\mu_B^2 \frac{\mu_0}{4\pi} \langle r^{-3} \rangle \frac{\langle 0 | \Lambda_i | 1 \rangle \langle 1 | N_i | 0 \rangle}{E_0 - E_1}. \quad (2)$$

The external field  $\mathbf{B}$  was parallel to the  $a$  or  $c$  crystallographic axes in our experiments, but in order to deal with the unknown relative orientation of the defect site's local principal axes, it is useful to convert to a reference frame of spherical coordinates in which

$$\mathbf{B} = B[(\sin \theta \cos \Phi)\mathbf{i} + (\sin \theta \sin \Phi)\mathbf{j} + (\cos \theta)\mathbf{k}]. \quad (3)$$

The calculated value of the nuclear shielding parameter  $\alpha$  is 0.08 for the optically excited  ${}^5D_0$  state and is not expected to vary dramatically from site to site. That is, the  ${}^5D_0$  shielding is quite small, and for the initial fit to the hole-burning data it was taken to be zero. The eigenvalues of the above Hamiltonian for the  $I = 5/2$  states associated with  ${}^5D_0$  therefore depend on just four site-dependent parameters:  $P$  and  $\eta$ , which are determined in zero field, and the unknown angles  $\theta$  and  $\Phi$ .

#### Line 41 (516 635 GHz)

The zero-field results give the following parameters for the excited  ${}^5D_0$  state:

${}^{151}\text{Eu}$ ,

$$P = 16.5 \pm 0.3 \text{ MHz}, \\ \eta = 0.43 \pm 0.05;$$

${}^{153}\text{Eu}$ ,

$$P = 42.4 \pm 0.3 \text{ MHz}, \\ \eta = 0.44 \pm 0.05.$$

In an applied field, separate best-fit values of  $\theta$  and  $\Phi$  were obtained for fields parallel to the crystallographic  $a$  and  $c$  axes. The hole-burning data for  $\mathbf{B}$  parallel to  $c$  are shown in Fig. 2 along with the results of that fit. The fitted angles for each case are

$$\mathbf{B} \parallel c: \theta = 75^\circ \pm 3^\circ, \quad \Phi = 48^\circ \pm 3^\circ,$$

$$\mathbf{B} \parallel a: \theta = 47^\circ \pm 3^\circ, \quad \Phi = 75^\circ \pm 3^\circ.$$

The fits to the data were quite satisfactory. Of the two angles  $\theta$  and  $\Phi$ , only the angle  $\theta$  can be related to the vanadate crystal axes. The two results for  $\theta$  are compatible and correspond to the quadrupole axis orientation shown in Fig. 3. The value of  $\theta = 47^\circ$  is also consistent with the lack of observable inequivalence splittings in the electronic Zeeman spectrum of this line for  $\mathbf{B} \parallel a$  (see Ref. 4 for a discussion of inequivalence splittings).

#### Line 44 (515 980 GHz)

The zero-field results give the following parameters for the excited  ${}^5D_0$  state<sup>1</sup>:

${}^{151}\text{Eu}$ ,

$$P = 10.2 \pm 0.1 \text{ MHz}, \\ \eta = 0.81 \pm 0.05;$$

${}^{153}\text{Eu}$ ,

$$P = 25.8 \pm 0.2 \text{ MHz}, \\ \eta = 0.81 \pm 0.05.$$

These are values given for line 30 in the earliest  $\text{EuVO}_4$  study<sup>1</sup>; this line occurs at the same frequency as and has a

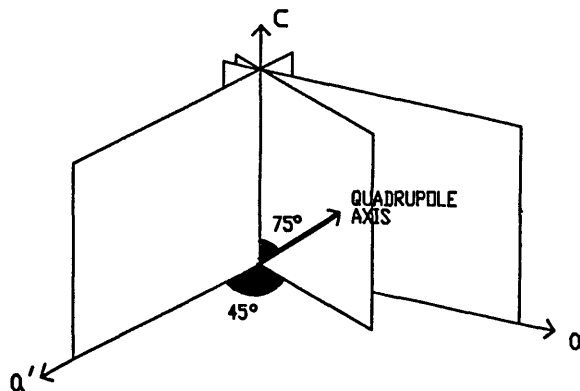


Fig. 3. Nuclear quadrupole axis orientation for line 41, with reference to the crystallographic axes, as determined from analysis of the Zeeman effect of the spectral hole burning for line 41.

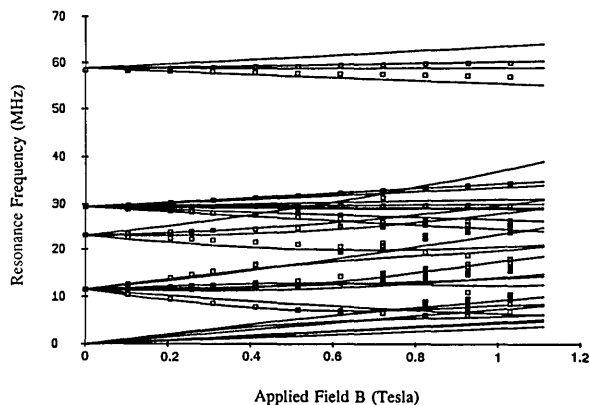


Fig. 4. Zeeman effect of the  ${}^7F_0$  ODNQR data for line 41 with the magnetic field  $\mathbf{B}$  applied parallel to the crystallographic  $c$  axis (squares). The theoretical fit (solid lines) was made by using the adjustable parameters  $P$  and  $\eta$  determined for  ${}^7F_0$  and the angles  $\theta$  and  $\Phi$  determined from the Zeeman effect of the  ${}^5D_0$  spectral hole burning for line 41.

hole-burning pattern identical to that of line 44 in this study. The best-fit values for  $\theta$  and  $\Phi$  also come from the previous study,<sup>1</sup> where, because the field was applied parallel to  $c$  only, the result was ambiguous; there are two pairs of  $\theta$  and  $\Phi$  that give acceptable fits to the data:

$$\begin{aligned}\theta &= 83^\circ \pm 5^\circ, & \Phi &= 27^\circ \pm 5^\circ; \\ \theta &= 66^\circ \pm 5^\circ, & \Phi &= 0^\circ \pm 5^\circ.\end{aligned}$$

It is shown below that analysis of the Zeeman ODNQR spectra permits a choice to be made between these two results.

#### Zeeman Optically Detected Nuclear Quadrupole Resonance Results

All resonance lines observed in these experiments were attributable to  $I = 5/2$  nuclear eigenstates associated only with the  ${}^7F_0$  ground state. While resonance lines attributable to nuclear eigenstates of the optically excited state should be observable, such resonances were too weak to be seen in the present experiments. The ODNQR data therefore represent a valuable complement to the hole-burning data; the hole-burning results were straightforward to interpret only for the *optically excited state* in this case.

In again seeking a best-fit of the Zeeman ODNQR data to Hamiltonian parameters, it is important to realize that the nuclear shielding factor  $\alpha$  that was near zero for the excited state  ${}^5D_0$  is much larger for the electronic ground state  ${}^7F_0$ , being equal to 0.78 for the intrinsic site parameters in  $\text{EuVO}_4$ .<sup>4</sup>

#### Line 41 (516 635 GHz)

Figure 4 shows the experimental ODNQR spectrum for line 41 as a function of magnetic field parallel to  $c$ . Attempts to fit these data with the shielding factor  $\alpha = 0.78$  (calculated for the intrinsic site) proved to be completely unsuccessful. The splittings in field are too large to be compatible with such a large  $\alpha$ , even assuming that a principal axis of the quadrupole tensor is aligned exactly parallel to the magnetic field ( $\theta = 0^\circ, \Phi = 0^\circ$ ). However, by using the values of  $\theta$  and  $\Phi$  already determined from the Zeeman hole-burning data, it was found that a value of

$\alpha = 0.42 \pm 0.01$  gave a good fit, as shown by the solid lines in Fig. 4. Various other values for  $\theta, \Phi$ , and  $\alpha$  were tried, since the form of the nuclear quadrupole Zeeman Hamiltonian shows that the three are not strictly independent, but the result shown in Fig. 4 was clearly the best fit to the data. In assessing the quality of fit in Fig. 4 (and in Fig. 5 below), it is necessary to note that the ODNQR lines have varied intensities, depending on details of the nuclear eigenstates, and that some lines are not observable. Strictly speaking, three separate values of  $\alpha$  should be used, since the large crystal field splittings apparently associated with these sites would result in a large anisotropy; time-resolved site-selective fluorescence experiments<sup>4</sup> are providing information on these crystal field splittings so that more-sophisticated analyses can be made. For  $\alpha$  values and angles outside the ranges quoted, however, the field dependence rapidly becomes qualitatively different. The basic results are thus clear.

#### Line 44 (515 980 GHz)

Figure 5 shows the experimental ODNQR spectrum for line 44, again for the field parallel to  $c$ . Once again the fit to the data was extremely unsatisfactory for  $\alpha = 0.78$ . With the  $(\theta, \Phi)$  determination given in the earlier study,<sup>1</sup> an attempt to fit the data with the  $(\theta, \Phi) = (83^\circ, 27^\circ)$  pair required a value of  $\alpha$  near zero, so those values were discounted as being nonphysical. For the second pair  $(66^\circ, 0^\circ)$ , however, a very good fit was achieved for a value of  $\alpha = 0.43 \pm 0.01$ , as can be seen from the solid lines in Fig. 5.

The surprising values for the nuclear shielding factor  $\alpha$  for lines 41 and 44 are not unprecedented. For 0.25%  $\text{Eu}^{3+}:\text{YAlO}_3$ , investigated previously,<sup>7,8</sup>  $\alpha$  was found to be highly anisotropic, with  $\alpha_z = 0.47$ . From the expression for  $\alpha$  given above the most likely difference between  $\alpha = 0.78$  for the intrinsic  $\text{Eu}^{3+}$  site and the  $\alpha = 0.42$  and  $\alpha = 0.43$  found for lines 41 and 44, respectively, is a change in the  ${}^7F_0$ - ${}^7F_1$  splitting caused by crystallographic distortion at the defect sites. However, the smaller values of  $\alpha$  imply splittings increased by nearly a factor of 2. This in turn would imply appreciable  $J$  mixing among the low-lying  $J$  states in  ${}^7F_J$ . For this reason, for any future attempt at a complete description of these two defect

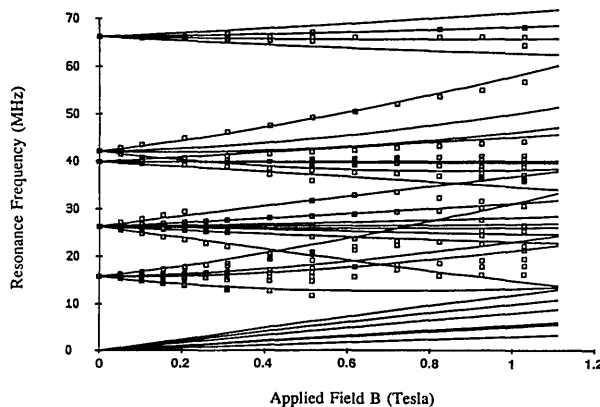


Fig. 5. Zeeman effect of the  ${}^7F_0$  ODNQR data for line 44 with the magnetic field  $\mathbf{B}$  applied parallel to the crystallographic  $c$  axis (squares). The theoretical fit (solid lines) was made by using the adjustable parameters  $P$  and  $\eta$  determined for  ${}^7F_0$  and the angles  $\theta$  and  $\Phi$  determined from the Zeeman effect of the  ${}^5D_0$  spectral hole burning for line 44.

sites, a simple perturbative approach to the crystal field effects of distortion will almost certainly prove to be inadequate. As is noted above, time-resolved site-selective fluorescence experiments are providing information on the crystal field splittings for these two sites and for others.<sup>4,6</sup>

## SUMMARY

Analyses of several of the defect sites in  $\text{EuVO}_4$  have been carried out by using the high-resolution techniques of ODNQR and spectral hole burning in applied magnetic fields. Important conclusions about the origin of these sites have been reached, with one site present only when fluoride contamination is present and one site present even in the cleanest crystals. These studies are being continued, and other  $\text{Eu}^{3+}$  lines in  $\text{EuVO}_4$  have been studied in similar detail<sup>4</sup>; those results are being combined<sup>4</sup> with (i) a thorough survey of the effect of changing the crystal growth parameters,<sup>4</sup> (ii) time-resolved site-selective emission spectroscopy,<sup>4,6</sup> and (iii) crystal field analyses.<sup>4,6</sup> Complete angular dependences of many of the magnetic field properties are being measured in the next series of experiments in order to extract even more detailed information about the defect sites.

## ACKNOWLEDGMENTS

We thank Barbara Wanklyn and B. E. Watts for growing the  $\text{EuVO}_4$  crystals. This research was supported in part by the Science and Engineering Research Council of the UK, NATO Collaborative Research grant CRG 910031, the Research Corporation, and the National Science Founda-

tion/Experimental Program to Stimulate Competitive Research (Montanans on a New Trak for Science).

\*Permanent address, Department of Physics, Montana State University, Bozeman, Montana 59717.

## REFERENCES

1. R. L. Cone, R. T. Harley, and M. J. M. Leask, "Nuclear quadrupole optical hole burning in stoichiometric  $\text{EuVO}_4$ ," *J. Phys. C* **17**, 3101-3111 (1984).
2. R. L. Cone, M. J. M. Leask, M. G. Robinson, and B. E. Watts, "Nuclear quadrupole optical hole burning in stoichiometric  $\text{EuAsO}_4$ ," *J. Phys. C* **21**, 3361-3380 (1988).
3. P. C. Hansen, M. Lazzouni, M. J. M. Leask, B. M. Wanklyn, and B. E. Watts, "Nuclear quadrupole holeburning in preparation-dependent  $\text{EuVO}_4$ ," *J. Phys. (Paris)* **49**, C8-889-C8-890 (1988).
4. P. C. Hansen, "Laser spectroscopy of rare earth ions," D.Ph. dissertation (University of Oxford, Oxford, 1990); R. L. Cone, P. C. Hansen, M. J. M. Leask, and R. M. Wanklyn, "Excitation spectra of flux-grown stoichiometric europium vanadate crystals," submitted to *J. Phys. Condensed Matter*.
5. R. M. Macfarlane and R. M. Shelby, "Coherent transient and holeburning spectroscopy of rare earth ions in solids," in *Spectroscopy of Crystals Containing Rare-Earth Ions*, A. A. Kaplyanskii and R. M. Macfarlane, eds. (North-Holland, Amsterdam, 1987), pp. 51-184.
6. Yongchen Sun, R. L. Cone, M. J. M. Leask, and M. M. Abraham, "Structure of defect sites in europium vanadate via optically detected nuclear resonance, spectral hole burning, and time-resolved fluorescence," submitted to *Phys. Rev. B*.
7. L. E. Erickson and K. K. Sharma, "Nuclear quadrupole resonance measurements of the anisotropic magnetic shielding and quadrupole coupling constants of  $^{151}\text{Eu}$  and  $^{153}\text{Eu}$  dilute in  $\text{YAlO}_3$  single crystal," *Phys. Rev. B* **24**, 3697-3700 (1981).
8. R. M. Shelby and R. M. Macfarlane, "Measurement of anomalous nuclear magnetic moment of trivalent Eu," *Phys. Rev. Lett.* **47**, 1172-1175 (1981).